Int. J. Heat Mass Transfer. Vol. 21, pp. 109–118. Pergamon Press 1978. Printed in Great Britain

HEAT TRANSFER TO FALLING LIQUID FILMS AND FILM BREAKDOWN—II

SATURATED LIQUID FILMS WITH NUCLEATE BOILING

TOSHIHIKO FUJITA* and TATSUHIRO UEDA
Department of Mechanical Engineering, University of Tokyo,
7-3-1 Hongo, Bunkyo-ku, Tokyo 113, Japan

(*Received* 10 *September* 1976)

Abstract—A series of boiling heat-transfer experiments is performed on saturated water films flowing on an inner tube of a vertically arranged annulus at atmospheric pressure. Data on heat-transfer coefficient and liquid droplet rate entrained by boiling are presented in a range of heat fluxes up to film breakdown. Taking into account characteristics of the droplet rate, variation of liquid film flow rate along the heating surface and film breakdown conditions are discussed.

NOMENCLATURE

c_p, specific heat;
D, inside diameter of outer tube;
d_0, outside diameter of heating tube;
h_c, forced convective heat-transfer coefficient;
h_{fg}, latent heat of vapourization;
h_i, heat-transfer coefficient, $h_i = q_0/\Delta t_s$;
h_i^*, dimensionless heat-transfer coefficient,

$$h_i^* = \frac{h_i}{k}\left(\frac{\nu^2}{g}\right)^{1/3};$$

k, thermal conductivity;
L, length of heating tube;
N, number of bursting bubbles per unit time and unit area of heating surface;
Pr, Prandtl number, $Pr = \mu c_p/k$;
q, heat flux;
q_B, film breakdown heat flux;
Re, film Reynolds number, $Re = 4\Gamma_f/\mu$;
t, temperature;
Δt_s, wall superheat;
u, velocity;
x, distance from upper end of heating tube;
y_i, mean film thickness.

Greek symbols

Γ, mass flow rate per unit periphery of heating tube;
μ, viscosity, $\mu = \rho\nu$;
ρ, density.

Subscripts

d, droplet;
f, liquid film;
g, steam;
in, upper end of heating tube, $x = 0$;
m, average over whole heating tube length;
o, outer surface of heating tube;
out, lower end of heating tube, $x = L$.

* Present address: Tokyo University of Mercantile Marine, 2-1-6 Echujima, Koto-ku, Tokyo 135, Japan.

1. INTRODUCTION

SEVERAL studies [1, 2] have been made on heat transfer to falling liquid films and breakdown of the films associated with increasing heat flux, in order to improve the efficiencies of some chemical industrial equipments and to examine the heat removal rate in cooling of nuclear fuel elements by falling films. The breakdown of saturated liquid films has also been investigated in relevant to the critical heat flux of high quality boiling in channels [3]. However, accumulation of the heat-transfer data of boiling films is insufficient and further study is needed to make clear the process leading to the film breakdown.

For subcooled water films, the authors have presented the experimental results of heat-transfer coefficient and film breakdown heat fluxes in Part I [4], and derived a distortion parameter of liquid films to correlate the film breakdown data.

In this study, boiling heat-transfer experiments are carried out for saturated water films flowing downwards on a heated tube at atmospheric pressure. The heat-transfer coefficient and droplet rate entrained by boiling are measured in a range of heat fluxes up to film breakdown. The breakdown process of boiling water films is quite different from that of subcooled films. This discrepancy is caused by the fact that the surface of boiling films is maintained at a temperature close to the saturation condition and there can be no variation of surface tension along the film. By this reason, the film breakdown heat flux of boiling films is much higher than that of distorted subcooled films.

2. EXPERIMENTAL EQUIPMENT AND PROCEDURE

The apparatus used in the present experiments is similar to the one shown in Part I [4]. The test section is an annulus as illustrated in Figs. 1(a) or (b). The core tube, which is installed concentrically inside a vertical glass tube covered with glasswool thermal insulators, consists of the water inlet section, intake region and heating section. The heating section is a stainless steel tube of 16 mm O.D., 0.93 mm thickness

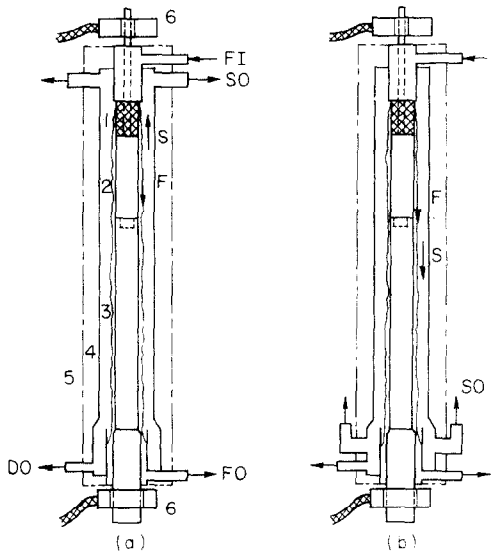

FIG. 1. Schematic diagram of test section: 1, sinter; 2, intake tube; 3, heating tube; 4, glass tube; 5, thermal insulators; 6, copper connections; F, liquid film flow; FI, liquid inlet; FO, liquid outlet for measuring film flow rate; S, steam flow; SO, steam outlet; DO, liquid outlet for measuring entrained droplet rate.

and 600 or 1000 mm length. A 250 mm length copper tube of the same diameter as the heating section is brazed at the upper end of the heating section as the intake region of film flow. At the water inlet section, a porous sinter tube of 70 mm length is provided to form a circumferentially uniform liquid film.

De-ionized water of electrical resistances greater than $5 \times 10^5\ \Omega \cdot$cm was used as the test liquid, and the core stainless steel tube was heated by passing a low voltage alternative current directly through the tube wall. The steam generated in the test section (a) was led upwards the annular channel in a direction opposite to film flow and released to the open air, while the steam in (b) was led downwards in parallel with film flow.

Table 1 gives dimensions of test sections and ranges of parameters covered experimentally. Heat flux was permitted up to 3.1×10^5 W/m^2 with a power supply used in the present experiments.

The inlet water temperature and flow rate were first adjusted to a set of values, and power supplied to the heating section was increased with a small increment. The power was kept constant for about 7 min at each level, and then measurements of the wall temperatures, outlet film flow rate and liquid droplet rate were carried out. This procedure was repeated until the film breakdown heat flux was reached. For measuring the wall temperatures, a thermocouple cluster was used similar to the one described in Part I. The liquid droplet rate was, as almost all of the droplets entrained by boiling were deposited on the outer tube, measured by collecting the liquid which flowed down the outer glass tube.

The liquid films under investigation reached the saturation temperature always within a short distance from the upper end of the heating tube. Hence, such distortion of film flow as that described in Part I was not observed along the tube periphery.

3. HEAT TRANSFER TO BOILING LIQUID FILMS

3.1. *Boiling curve*

Figure 2 shows an example of measured boiling curves for falling films of saturated water, where the heat flux q_w is plotted against the wall superheat $\Delta t_s = t_w - t_s$ for several inlet film flow rates $\Gamma_{f\,in}$. The data were obtained at a location of $x = 770$ mm, the temperature t_w is an average of heating surface temperatures which were obtained by correcting the measured values at three locations along the inner periphery of the tube taking into account the substantial temperature drops through the tube wall. The broken lines a and b in the figure show conditions of the incipient boiling for forced convective heat transfer, developed by Sato and Matsumura [5] and Bergles and Rohsenow [6] respectively. The range of wall superheats covered in the present experiments was higher than these values and nucleate boiling was observed over the whole range.

There have been few reports on boiling heat transfer to falling liquid films. Toda and Uchida [7] studied on boiling water films flowing horizontally at high velocities. The solid line A in Fig. 2 shows the empirical value presented by Toda and Uchida. The line B represents a correlation for fully developed nucleate flow boiling of water obtained by the empirical equation of McAdams *et al.* [8]

$$q_w = 2.26\Delta t_s^{3.86}\ \text{W/m}^2. \quad (1)$$

Table 1. Experimental conditions
(Heating section: 18-8 stainless steel tube, outside diameter 16 mm; wall thickness 0.93 mm; maximum heat flux: $q_w = 3.1 \times 10^5$ W/m^2)

Steam flow direction	Heating length L (mm)	Glass tube diameter D (mm)	Inlet water temperature $t_{f\,in}$ (°C)	Inlet film flow rate $\Gamma_{f\,in}$(kg/m·s)	Thermocouple locations x (mm)
Upward	1000	46	95.5	0.089–0.429	580, 770, 960
		31	87.5, 96.5	0.097–0.723	580, 770, 960
	600	31	95.5, 97.0	0.078–0.829	300, 440, 580
		25	88.0, 96.5	0.141–0.727	300, 440, 580
Downward	1000	31	95.5	0.095–0.351	580, 770, 960
	600	31	95.5	0.117–0.347	300, 440, 580
		25	95.5	0.118–0.352	300, 440, 580

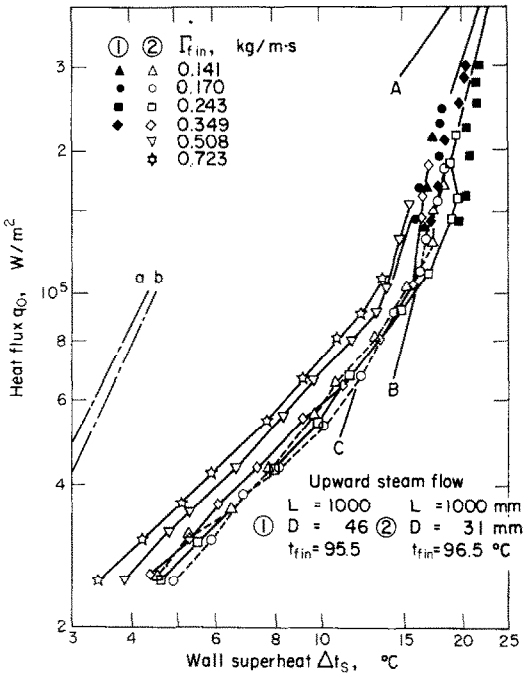

FIG. 2. Boiling curves for falling liquid films: A, Toda and Uchida [7]; B, McAdams *et al.*, equation (1); C, Nishikawa [9]; a, Sato and Matsumura [5]; b, Bergles and Rohsenow [6].

The line *C* shows a typical correlation for pool boiling developed by Nishikawa [9].

In boiling liquid films, vapour bubbles grew in a shape of a hemispherical dome and were carried down by the film flow. With an increase of heat flux, the bubbles increased in the formation rate and decreased in the travelling distance along the tube before bursting.

In a range of heat fluxes $q_o = (0.3\text{–}0.8) \times 10^5$ W/m^2, the density of bubble formation was insufficient to make much contribution to the boiling curves. Hence, the heat flux q_o is proportional to the wall superheat Δt_s, that is, the heat-transfer coefficient is dependent on the inlet film flow rates Γ_{fin}. As the decrease of film flow rate by evaporation and droplet entrainment was small in the range of heat fluxes, the local heat-transfer coefficient h_i could be easily correlated with the local film flow rate as is described later.

In a range of $q_o = (1.1\text{–}1.7) \times 10^5$ W/m^2, the rate of bubble formation became high and the bubbles grew rapidly and burst producing lots of liquid droplets. Most of the droplets were deposited on the surface of the outer glass tube and flowed down the surface as a film. The boiling curves in this range have a little more steeper gradient, and in a range above $q_o = 1.7 \times 10^5$ W/m^2, the curves show a trend well similar to the line *B*, equation (1) for forced convection nucleate boiling.

Experimental data obtained at the locations $x = 580$ and 960 mm and those obtained with different inlet water temperatures and tube length were also found to fall on the boiling curves shown in Fig. 2. Moreover, in the case where generated steam flowed down the annulus in parallel with film flow, boiling curves were also similar to those in the figure.

3.2. *Heat-transfer coefficient*

Figure 3 shows the result for heat-transfer coefficient h_i at the location $x = 770$ mm, plotted against film flow rate Γ_f for some different heat fluxes q_o. The flow rate Γ_f was determined, to an approximation, by interpolating the film flow rates measured at both ends of the heating section. The broken line in the figure shows the empirical correlation of heat-transfer coefficient

$$\left.\begin{aligned} h_i^* &= 0.606(Re/4)^{-0.22} && \text{for laminar regime} \\ h_i^* &= 3.8 \times 10^{-3} Re^{0.4} Pr^{0.65} && \text{for turbulent regime} \end{aligned}\right\} \quad (2)$$

which were presented by Chun and Seban [10] for evaporating water films flowing downwards on outside of a stainless steel tube.

In a range of heat fluxes $q_o = (0.3\text{–}0.7) \times 10^5$ W/m^2 where the population of bubble formation is low, our experimental values show a trend according to Chun and Seban, although the values are higher by about 10% than theirs. Our experimental values can be approximately fitted by the following equations for

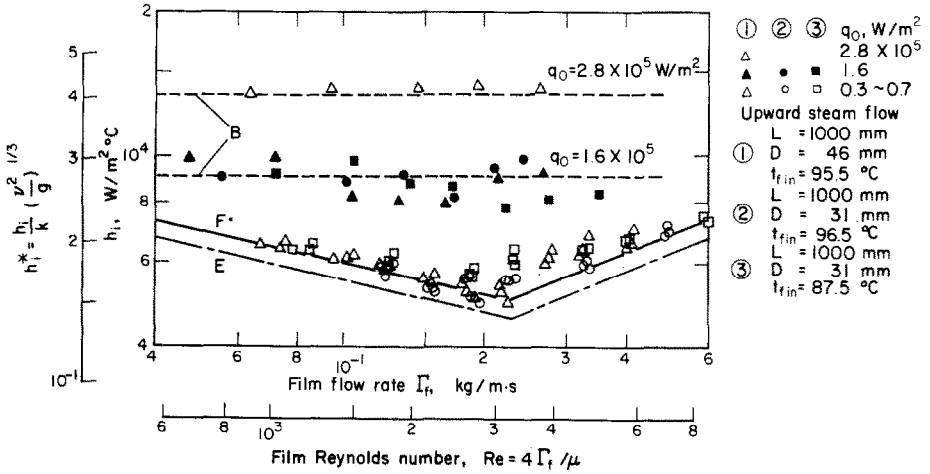

FIG. 3. Heat transfer coefficient to boiling liquid films: B, McAdams *et al.*, equation (1)′; E, Chun and Seban, equation (2); F, present study, equation (3).

water at atmospheric pressure:

$$\left.\begin{aligned} h_i^* &= 0.90\,Re^{-0.22} \quad \text{for} \quad Re < 3200 \\ h_i^* &= 6.0\times10^{-3}\,Re^{0.4} \quad \text{for} \quad Re \geqslant 3200. \end{aligned}\right\} \quad (3)$$

With an increase of heat flux, the effect of film flow rate on heat-transfer coefficient becomes less important. Although the data points are somewhat scattered at a heat flux $q_o = 1.6\times10^5\ \mathrm{W/m^2}$, the data points at $q_o = 2.8\times10^5\ \mathrm{W/m^2}$ are independent of the film flow rate, i.e. fully developed nucleate boiling. The dotted lines in the figure show the values obtained from an altered expression of equation (1)

$$h_i = q_o/\Delta t_s = 1.24 q_o^{0.741}\ \mathrm{W/m^2\,°C} \quad (1)'$$

which are in good agreement with the data points.

Therefore, in the fully developed nucleate boiling of falling films, where the formation and bursting of vapour domes are remarkable, the magnitude of heat transfer coefficient is found to be approximately equal to that in the fully developed flow boiling in a channel.

4. LIQUID DROPLET RATE ENTRAINED BY BOILING

The amount of liquid droplets arising from bursting of vapour bubbles is closely related to the boiling situation in liquid films. The liquid droplets are dispersed from the liquid film. This promotes the reduction of film flow rate and eventually the appearance of dry patches near the lower end of the heating tube. Petrovichev *et al.* [11] measured the rate of droplet entrainment resulting from nucleate boiling for water films flowing down a short stainless steel tube of 50 mm heating length. For the rate of droplet entrainment $(\Gamma_d)_L/L$, they proposed the following empirical relationship:

$$(\Gamma_d)_L/L = A y_i (q_o - q_{ei})^{2.7}\ \mathrm{kg/m^2 s} \quad (4)$$

where y_i denotes the film thickness (mm), q_o heat flux ($\mathrm{W/mm^2}$), $q_{ei} = 0.15\ \mathrm{W/mm^2}$ is the heat flux at inception of entrainment and $A = 2.09$. Their measurement covered the ranges $\Gamma_f = 0.22$–$0.56\ \mathrm{kg/m\cdot s}$ and $q_o = 0.7$–$1.5\ \mathrm{W/mm^2}$.

4.1. *Results of entrained droplet rate*

Figure 4 shows an example of the results, plotted the droplet rate averaged over the whole heating length $(\Gamma_d)_L/L$ against the heat flux q_o. It is found from this figure that the droplet rate increases rapidly with increasing heat flux, satisfying fairly well the relation $(\Gamma_d)_L/L \propto q_o^{2.5}$.

The droplet rate is also found to increase with increasing film flow rate. Figure 5 shows the result plotted against the averaged film flow rate over $\Gamma_{fm} = (\Gamma_{fin} + \Gamma_{fout})/2$. The data points show a trend to satisfy the relation $(\Gamma_d)_L/L \propto \Gamma_{fm}^{0.5}$. Since the mean thickness of a falling film y_i is related approximately by the expression $y_i \propto \Gamma_{fm}^{0.5}$ in this flow rate range [12], the droplet rate is supposed to be nearly proportional to the film thickness.

On the basis of these results, the data of entrained droplet rate are plotted against the group $\Gamma_{fm}^{0.5} q_o^{2.5}$ as shown in Fig. 6. As is evident from this figure, the mean entrained droplet rate can be expressed, regardless of heating lengths $L = 600$ and 1000 mm and of steam flow directions, as follows:

$$(\Gamma_d)_L/L = C\Gamma_{fm}^{0.5} q_o^{2.5} \quad (5)$$

where $C = 5.3\times10^{-15}(\mathrm{kg\cdot m^7/W^5 s})^{0.5}$.

The droplet rate $(\Gamma_d)_L/L$ of equation (4) was derived from the data for the heat fluxes much higher than ours. In spite of this, the trend of $(\Gamma_d)_L/L$ against both q_o and Γ_f seems to be similar to ours, although the

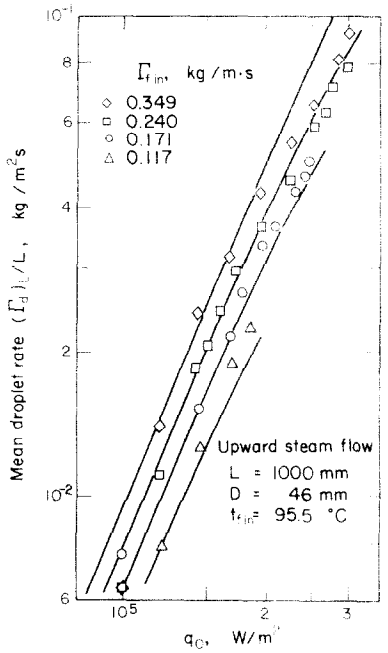

FIG. 4. Effect of heat flux on droplet rate.

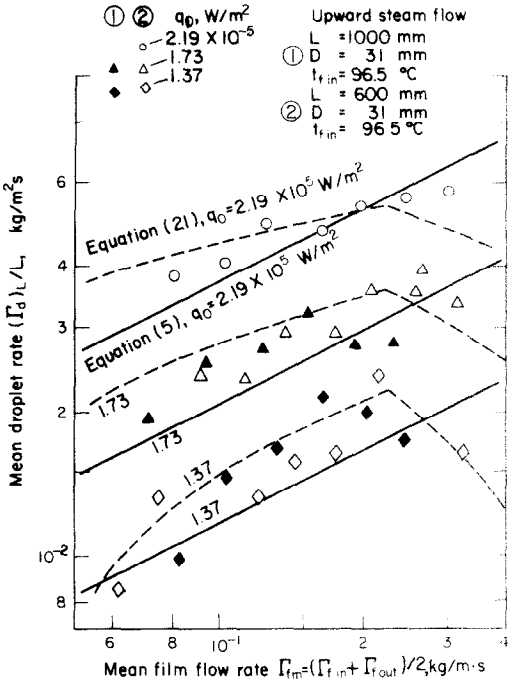

FIG. 5. Effect of film flow rate on droplet rate.

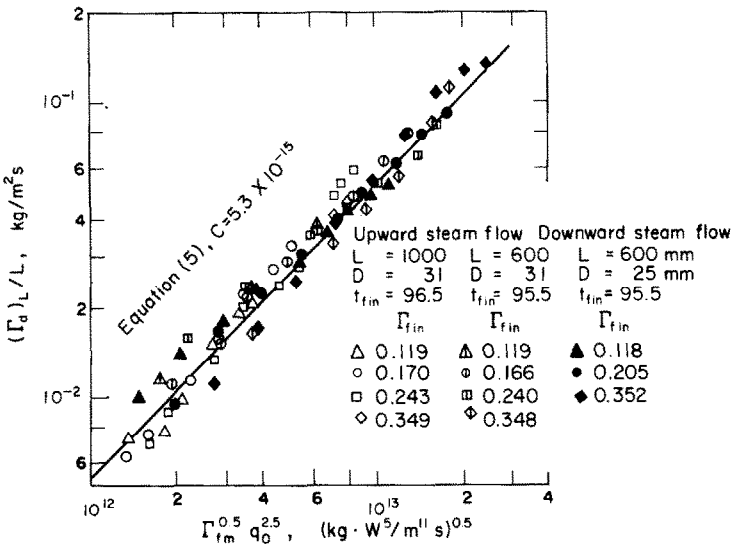

FIG. 6. Mean droplet rate in terms of mean film flow rate and heat flux.

value of $(\Gamma_d)_L/L$ appears to be rather small due to that the measurement was carried out in a thermal entrance region.

4.2. *Calculation of local film flow rate*

As is illustrated in Fig. 7, a mass balance for an increment of length dx of unit film width can be written in terms of evaporation and droplet entrainment as follows:

$$\frac{d\Gamma_f}{dx}+\frac{d\Gamma_g}{dx}+\frac{d\Gamma_d}{dx}=0. \tag{6}$$

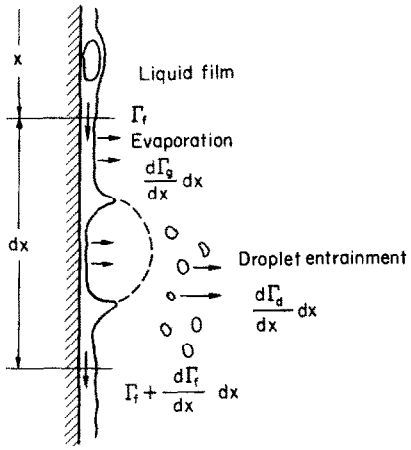

FIG. 7. Mass balance of a boiling liquid film.

When a liquid film has already reached the saturation temperature, the evaporation rate per unit area is proportional to the heat flux;

$$\frac{d\Gamma_g}{dx}=\frac{q_o}{h_{fg}}. \tag{7}$$

Referring to equation (5), the entrained droplet rate per unit area can be expressed as

$$\frac{d\Gamma_d}{dx}=C\Gamma_f^{0.5}q_o^{2.5}. \tag{8}$$

By substituting equations (7) and (8) into (6), the following differential equation is obtained.

$$\frac{d\Gamma_f}{dx}+\frac{q_o}{h_{fg}}+C\Gamma_f^{0.5}q_o^{2.5}=0. \tag{9}$$

Denoting the location where the film reaches the saturation temperature as x_s, and the film flow rate at the location as Γ_{fs}, above equation is integrated from x_s to x under the constant heat flux condition;

$$\Gamma_f^{0.5}-A\ln|\Gamma_f^{0.5}+A|=\Gamma_{fs}^{0.5}-A\ln|\Gamma_{fs}^{0.5}+A|-B(x-x_s) \tag{10}$$

where $A=1/Ch_{fg}q_o^{1.5}$ and $B=Cq_o^{2.5}/2$.

In calculating the film flow rate Γ_{fs} at the location x_s, the evaporation rate in the subcooled film region can be ignored. But, since the droplet entrainment arises from bursting of bubbles produced by subcooled boiling, the droplet rate must be taken into account. Approximating the droplet rate by equation (8) and substituting this into equation (6),

$$\frac{d\Gamma_f}{dx}+C\Gamma_f^{0.5}q_o^{2.5}=0. \tag{11}$$

Denoting the film flow rate at the upper end of the heating section $x=0$ as Γ_{fin}, this equation is integrated from 0 to x_s;

$$\Gamma_{fs}^{0.5}=\Gamma_{fin}^{0.5}-Bx_s, \tag{12}$$

Substituting this into equation (10), the following expression can be obtained.

$$\Gamma_f^{0.5}-A\ln|\Gamma_f^{0.5}+A|=\Gamma_{f\,in}^{0.5}-A\ln|\Gamma_{f\,in}^{0.5}+A-Bx_s|-Bx \tag{13}$$

where x_s can be approximated by

$$x_s=c_p\Gamma_{f\,in}(t_s-t_{f\,in})/q_o. \tag{14}$$

Therefore, the local film flow rate Γ_f can be calculated by applying a simple iteration method to equations (13) and (14), for given inlet water temperature $t_{f\,in}$, inlet film flow rate $\Gamma_{f\,in}$ and heat flux q_o. Then, the droplet entrainment from an arbitrary length x of

Table 2. Characteristics of boiling bubbles in falling films (Heating length $L = 600$ mm; glass tube diameter $D = 31$ mm, upward steam flow)

Cine film number		(1)	(2)	(3)	(4)	(5)
Inlet film flow rate						
$\Gamma_{f\,in}$	(kg/m·s)	0.419	0.240	0.240	0.223	0.139
Inlet water temperature						
$t_{f\,in}$	(°C)	94.5	96.3	93.7	95.2	95.9
Heat flux						
q_o	(W/m^2)	1.94×10^5	1.93×10^5	2.22×10^5	1.67×10^5	1.67×10^5
Outlet film flow rate						
$\Gamma_{f\,out}$	(kg/m·s)	0.342	0.169	0.156	0.165	0.085
Entrained droplet rate						
$(\Gamma_d)_L$	(kg/m·s)	0.028	0.026	0.031	0.020	0.017
Wall superheat						
Δt_s	(°C)	21.5 (440)	22.7 (440)	17.4 (440)	18.5 (440)	20.1 (440)
Measuring section						
x	(mm)	(380–420)	(380–420)	(410–440)	(440–480)	(440–480)
Measuring time						
	(ms)	109	174	117	193	248
Bubble formation rate						
N	(l/m^2 s)	6.12×10^5	4.46×10^5	1.29×10^6	4.85×10^5	1.67×10^5
Mean bursting diameters						
$\bar{d}_b/(\overline{d_b^3})^{1/3}$	(mm)	5.30/5.94	5.95/7.02	5.19/5.86	5.33/6.46	6.37/7.70
Heat flux						
q_b'	(W/m^2)	4.52×10^4	5.44×10^4	9.18×10^4	4.61×10^4	2.91×10^4
Film flow rate						
Γ_f	(kg/m·s)	0.368 (400)	0.193 (400)	0.181 (425)	0.179 (460)	0.098 (460)
Heat flux						
q_b	(W/m^2)	6.4×10^4	7.6×10^4	1.30×10^5	7.0×10^4	4.7×10^4
Ratio						
q_b'/q_b		0.71	0.72	0.71	0.66	0.62

unit film width can also be calculated from

$$\Gamma_d = \Gamma_{f\,in} - \Gamma_f - q_o(x - x_s)/h_{fg}. \tag{15}$$

The solid lines in Fig. 4 show the entrained droplet rates calculated from above equations for given $\Gamma_{f\,in}$ under the conditions that $t_{f\,in} = 95.5$°C and $x = 1$ m. The trend of the data points in the figure is expressed well with these lines.

4.3. *Observation of boiling bubbles*

Vapour bubbles generated in a falling film on the heating surface were carried down by the film flow forming hemispherical domes until their bursting. The velocity of an individual falling bubble varied with time and position, but it was nearly equal, in average, to the mean liquid film velocity. The radius of the bubble increased rapidly in an initial growth period and was in proportion to a square root of time throughout its growth. This trend of the bubble growth rate is more or less similar to that shown, for example, by Plesset and Zwick [13] for a free spherical bubble in an initially uniformly superheated infinite liquid, and van Stralen *et al.* [14] for a hemispherical bubble surrounded by two sorts of initially superheated microlayers. At low bubble densities where vapour bubbles formed discretely, the bubbles were seen to burst either by itself or by touching the outer tube surface, whereas at high bubble densities, most of the bubbles were seen to burst one after another being perforated by collisions with droplets dispersed from adjacent bursting bubbles.

Table 2 shows the results obtained from high speed cine films, where $\bar{d}_b$ and $(\overline{d_b^3})^{1/3}$ are the mean diameters of bubbles just before being perforated and N is the number of bubbles bursting per unit time and unit area of the heating surface. As shown in the table, the number of bursting bubbles N increases rapidly with increasing heat flux. The number N also increases with increasing film flow rate, but the diameter of bursting bubbles decreases.

Here, estimate the heat flux spent for bubble formation q_b. The heat flux at the wall surface q_o is expressed by a superposition of q_b and the heat flux due to forced convection q_c which is conveyed across a liquid film and removed away from the film surface by vapourization,

$$q_o = q_b + q_c.$$

Although the heat flux q_c is more or less influenced by formation and bursting of bubbles, suppose q_c may be approximated by the heat flux in evaporating films without nucleation,

$$q_c = h_c \Delta t_s, \tag{16}$$

Then,

$$q_b = q_o - h_c \Delta t_s \tag{17}$$

where h_c denotes the heat-transfer coefficient to evaporating falling films.

The heat flux q_b in Table 2 was calculated from this equation (17), by using the measured q_o and Δt_s, and

the heat-transfer coefficient h_c evaluated from equation (3). Another heat flux q_b' is shown in the table, which was calculated from the following equation by assuming that the shape of an individual bubble is a right hemisphere:

$$q_b' = \frac{\pi}{12}\overline{d_b^3}\rho_g h_{fg} N. \tag{18}$$

Now compare the value of heat flux q_b' with q_b. The experimental results show that $q_b'/q_b = 0.62$–0.72. However, taking into account that each bubble dome is rather inflated than a right hemisphere and that some miscount of the bubble number is unavoidable because some bubbles may be overlapped around a circular tube, the heat flux q_b' is supposed to be approximately equal to the heat flux q_b. That is, the heat flux q_b calculated from equation (17) is possibly regarded as the heat flux to be spent for bubble formation.

4.4. *Consideration on droplet entrainment*

In this section, some considerations are added to the droplet entrainment rate arising from bursting of vapour domes.

Here, denoting the number of bubbles bursting per unit time and unit area of a heating surface as N, the mean volume of the bubbles as V_b, and the mean volume of liquid droplets entrained by bursting of one bubble as V_d, the entrained droplet rate $d\Gamma_d/dx$ can be expressed as follows:

$$d\Gamma_d/dx = \rho V_d N. \tag{19}$$

By introducing the heat flux spent for bubble formation q_b, the bubble number is written in the form

$$N = q_b/h_{fg}\rho_g V_b. \tag{20}$$

Therefore,

$$\frac{d\Gamma_d}{dx} = \frac{q_b}{h_{fg}\rho_g}\frac{\rho}{V_b}\frac{V_d}{} = \frac{q_o - h_c\Delta t_s}{h_{fg}}\frac{\rho}{\rho_g}\frac{V_d}{V_b}. \tag{21}$$

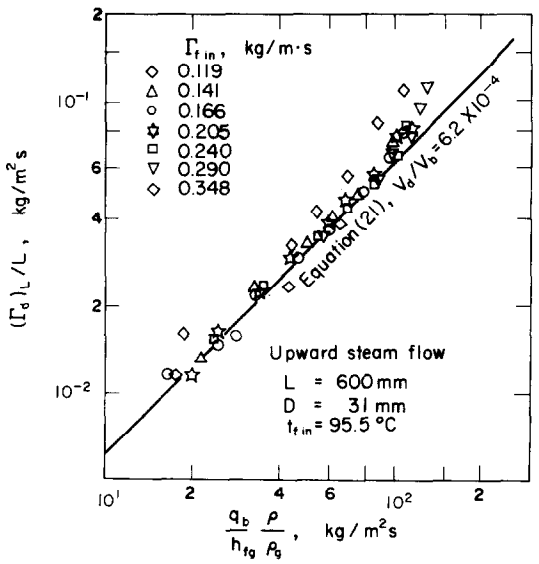

FIG. 8. Droplet rate correlated with the heat flux spent for bubble formation.

Figure 8 shows an example of the results plotted the entrained droplet rate $(\Gamma_d)_L/L$ against the value of

$$\frac{q_b}{h_{fg}}\frac{\rho}{\rho_g}.$$

It will be seen that the data points fall on the straight line with a slope of 45° in a range of film flow rates less than 0.24 kg/m·s, and the value of V_d/V_b is expressed simply by

$$V_d/V_b \simeq 6.2 \times 10^{-4}.$$

However, as the mean diameter of bursting bubble has a trend to decrease with increasing film flow rate, the value of V_d/V_b may be affected by the film flow rate. It may be considered that the value of V_d/V_b is possibly affected also by fluid properties and conditions of heating surfaces.

The dotted lines in Fig. 5 show the entrained droplet rates estimated by equation (21) by means of Δt_s and h_c calculated from equations (1) and (3) and $V_d/V_b = 6.2 \times 10^{-4}$. In a range where film flow rates are low, the lines obtained in the way are in good agreement with experimental results of $(\Gamma_d)_L/L$. However, in a range above $\Gamma_{fm} = 0.23$ kg/m·s, the lines show a trend different from that of the experimental results.

5. FILM BREAKDOWN

5.1. *Modes of film breakdown*

In the present experiments made for evaporating liquid films with nucleate boiling, two modes of film breakdown were observed. One mode was due to the formation of large dry patches near the lower end of the heating section where the film flow rate had been decreased by vapourization and droplet entrainment. Another mode of breakdown was due to the flooding caused by upward steam flow near the upper end of the heating section, which was accompanied with a sudden reduction of the downward film flow rate on the heating surface. Once a film had broken down, the heating surface dried out soon and its temperature rose up rapidly. Hence, when a liquid film was supplied again to the dry surface from upstream, violent nucleate boiling took place at the film front and most of the liquid film was ejected at there by the sputtering action [2].

Figure 9 shows the results of film breakdown heat flux q_B plotted against inlet film flow rate $\Gamma_{f\,in}$, which were obtained under the condition that generated steam was flowing upwards. In this figure, the film breakdown due to large dry patch formation is mainly seen in a range where the inlet film flow rates are low. On the other hand, the film breakdown due to flooding is seen in a range of high film flow rates, and the film breakdown heat flux is strongly affected by outer tube diameters. Moreover, between the two modes of film breakdown, a transition region is observed in which the formation of large dry patches near the lower end of the heating section is promoted by the effect of upward steam flow on liquid film flow. Two solid lines added in the lower part of Fig. 9 show, for reference, the film breakdown heat fluxes for subcooled films of 20°C and 60°C, respectively.

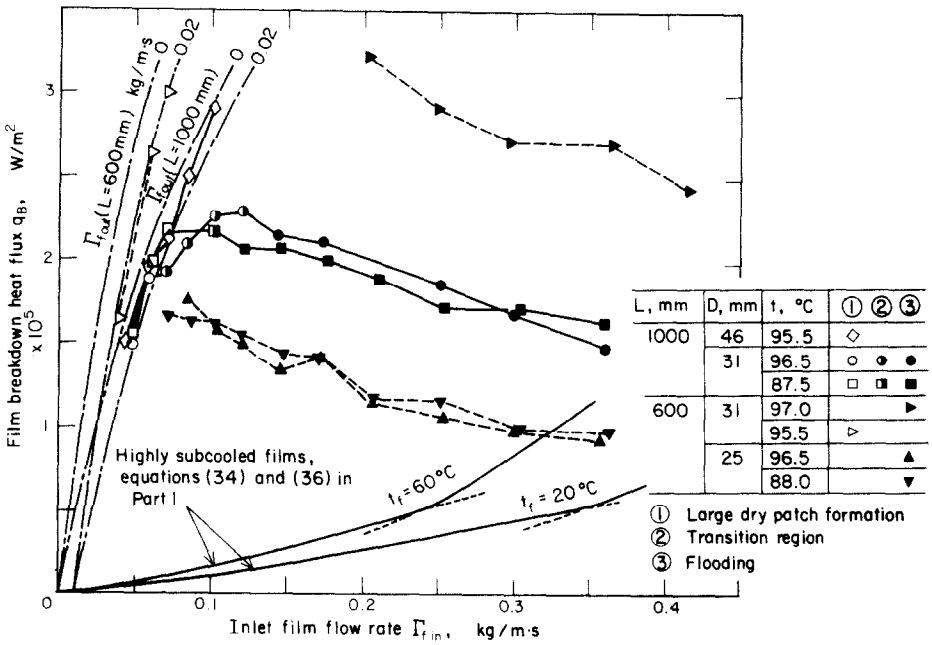

FIG. 9. Variation of film breakdown heat flux with inlet film flow rate.

5.2. *Film breakdown by dry patches*

When a vapour bubble burst, a small incipient dry patch was sometimes observed at a point where the bubble was initiated. This dry patch was soon rewetted by a liquid film flowing down the heating surface. With increasing heat flux and with decreasing film flow rate, the number of the intermittent dry patches increased and an individual dry patch became larger in its dimension and longer in its existence time. But, in such a condition, the temperature of the heating tube remained on the boiling curve described before, although it varied slightly with time and position. The rapid rising of the wall temperature did not occur until the dry surface came to occupy near a half width of the tube periphery as a result of several dispersed dry patches being joined together.

Figure 10 shows variation of the film flow rate measured at the lower end of heating section $\Gamma_{f\,out}$. When the heat flux $q_o = 0$, the flow rate at the lower end of heating section is of course equal to the inlet flow rate, $\Gamma_{f\,out} = \Gamma_{f\,in}$. The figure represents how the lower end flow rate decreases with increasing heat flux.

The data plotted by ● indicate the existence of small intermittent dry patches in the film, and the points plotted by □ show the film breakdown due to the formation of large dry patches accompanied with rapid rising of the wall temperature. The broken lines in the figure show the outlet film flow rate calculated from equation (13) with a value of $C = 5.3 \times 10^{-15}$, which are in good agreement with the experimental results. The dotted straight lines show the outlet flow rate calculated by assuming that the film flow rate is reduced only by evaporation. It is found that the droplet entrainment contributes to the reduction of film flow rate considerably in a range of high heat fluxes.

As is evident from this figure, the incipient dry patches appear at lower heat fluxes with a decrease of

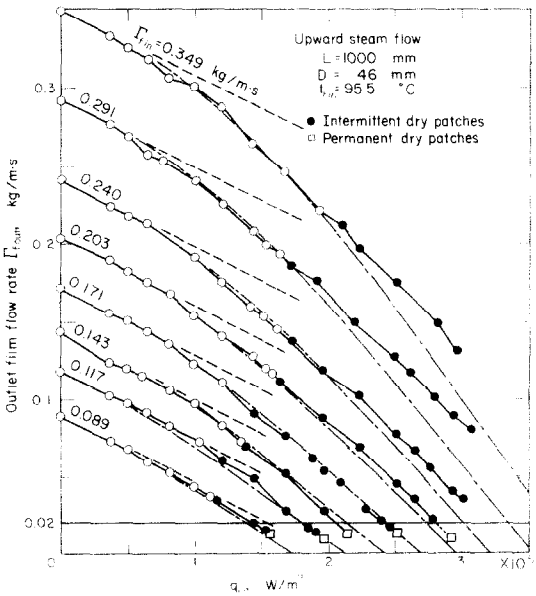

FIG. 10. Variation of outlet film flow rate with heat flux and formation of dry patches.

outlet film flow rate. When the outlet film flow rate attains a value in a range $\Gamma_{f\,out} = 0.01$–0.02 kg/m·s by a further increase of heat flux, large permanent dry patches are formed.

The other data obtained under the different conditions of the heating length, outer tube diameter and steam flow direction were all similar to those shown in Fig. 10, and the film breakdown due to large dry patches took place at a condition of $\Gamma_{f\,out} = 0.01$–0.02 kg/m·s.

The broken lines in Fig. 9 show the relations of heat flux q_o and inlet film flow rate $\Gamma_{f\,in}$, at conditions where outlet film flow rates attain values of $\Gamma_{f\,out} = 0$ and 0.02 kg/m·s. These were calculated from equation (13)

and a value of $C = 5.3 \times 10^{-15}$ for each heating length of $L = 600$ and 1000 mm. All of the film breakdown data due to large dry patch formation fall between the two lines for each heating length.

Formation of incipient dry patches. It has been reported that large hemispherical vapour domes are formed in nucleate pool boiling of thin liquid films, and that in some conditions intermittent dry patches appear on the heating surface beneath the domes [15]. In falling films, boiling bubbles also formed hemispherical domes. However, the diameter of the domes was rather small comparing with that in pool boiling, and dry patches were not initiated until the heat flux was increased to a higher value in falling films. This discrepancy will be ascribed to the effect of film motion. The incipient dry patches were first observed near the lower end of the heating section where the velocity of the liquid film had been lowered. From observation, it is considered that the appearance of an incipient dry patch is resulting from loss of a thin liquid layer beneath a vapour dome by evaporation.

Formation of permanent dry patches. In saturated falling films, large permanent dry patches were found to form near the lower end of the heating section, when the outlet film flow rate was reduced to a value in a range of $\Gamma_{f\,\mathrm{out}} = 0.01$–$0.02\,\mathrm{kg/m \cdot s}$ by an increase of heat flux. Then, consider a force balance at the upper end boundary of a large dry patch formed in a uniform laminar liquid film of flow rate $\Gamma_{f\,\mathrm{out}}$. Denoting the mean dynamic pressure of the film as P_d, the film thickness as y_i, the contact angle as ϕ', and the surface tension neglecting its variation with temperature as σ, then

$$P_d y_i = \sigma(1-\cos\phi') \tag{22}$$

where P_d and y_i are given, as shown in Part I, by the following equations including the film Reynolds number $Re = 4\Gamma_{f\,\mathrm{out}}/\mu$:

$$P_d/\rho g\left(\frac{\nu^2}{g}\right)^{1/3} = \frac{1}{15}\left(\frac{3}{4}\right)^{4/3} Re^{4/3}$$

$$y_i = \left(\frac{3}{4}\frac{\nu^2}{g} Re\right)^{1/3}.$$

For saturated water films of $\Gamma_{f\,\mathrm{out}} = 0.01$–$0.02\,\mathrm{kg/m \cdot s}$ which are corresponding to $Re = 140$–280, $y_i = 0.098$–0.12 mm and $P_d = 6.5$–$16\,\mathrm{N/m^2}$, equation (22) leads to the values of contact angle as

$$\phi' = 8.5\text{–}15°.$$

These superficial contact angles ϕ', which are determined by applying the values of $P_d y_i$ for uniform film flow, show considerably small values comparing with such actual contact angles ϕ of water on a stainless steel plate as, for example, $\phi = 66°$ given by Ponter *et al.* [16] and $\phi = 45°$ by Hartley and Murgatroyd [17]. The discrepancy between the two contact angles is considered to be caused by the fact that the actual value of the mean dynamic pressure term $P_d y_i$ varies with wave motion in the film and then the maximum value of the term $P_d y_i$ is possibly large enough to balance with the actual surface tension term $\sigma(1-\cos\phi)$ at the upper end boundary of the dry patch.

Norman and McIntyre [18] have measured the minimum liquid rate required to maintain a continuous film, and found the flow rate is approximately $\Gamma_f = 0.01\,\mathrm{kg/m \cdot s}$ for isothermal water films. Application of this result to equation (22) yields $\phi' \simeq 10°$. For water films flowing upwards on a acrylic regin tube, Hewitt and Lacey [19] have measured the minimum liquid rate at which a dry patch formed artificially is re-covered, and have shown that $\phi' = 17°$. These values of ϕ' are in accordance with those in the present study.

5.3. *Film breakdown by flooding*

In the present experiments, flooding originated near the place of highest steam velocity flowing upwards, that is, the position where a liquid film attained the saturation temperature. When the flooding condition is reached, large waves formed on the film are carried upwards by the steam flow, and slugs of liquid–vapour mixture are produced around the heating tube near the upper end and move up and down in the annular channel. The discontinuity of downward film flow thus produced leads to dryout of the heating surface and subsequent temperature rise of the tube wall.

In order to investigate the effects of various parameters on appearance of flooding, the experimental data plotted in Fig. 9 were converted into the relation between the maximum steam velocity and the liquid film velocity. The flooding velocity, i.e. the upward steam velocity required to cause flooding decreased with increasing liquid film velocity and decreasing outer tube diameter, in other words, the clearance of annular space. These trends are similar to those of flooding in two-component counter-current two-phase flow [20]. In the present experiments, however, the tube length had no effects on the flooding velocity. This is because flooding occurs always within a short distance below the upper end of the heating tube where the steam velocity attains a maximum value.

6. CONCLUSIONS

From the experimental results and discussion on heat-transfer coefficient, entrained droplet rate and film breakdown conditions for saturated water falling films, the following conclusions are obtained:

(1) In a range of low heat fluxes, the heat-transfer coefficient to a saturated boiling liquid film shows a trend similar to that of forced convection evaporation presented by Chun and Seban. While in a range of high heat fluxes where nucleate boiling is fully developed, it shows a value approximately equal to that of the forced convection nucleate boiling in channels.

(2) The liquid droplet rate arising from bursting bubbles is expressed by equation (8). Applying this equation, the variation of film flow rate is calculated along the heating tube. The results show a good agreement with the measured values.

(3) When the outlet film flow rate decreases to a value in a range $\Gamma_{f\,out} = 0.01$–$0.02\,kg/m \cdot s$, the film breakdown due to large dry patches and subsequent temperature rise take place near the lower end of the heating tube. The force balance at the upper end boundary of the dry patch leads to the superficial contact angles of $\phi' = 8.5$–$15°$.

(4) When the velocity of counter-current steam flow attains a certain value, flooding occurs at a position where the steam velocity comes near a maximum. This brings about rapid disappearance of the downstream liquid film and subsequent temperature rise of the tube wall. The flooding steam velocity becomes lower with increasing liquid film velocity and with decreasing the clearance of annular space.

REFERENCES

1. G. F. Hewitt and N. S. Hall-Taylor, *Annular Two-phase Flow*, Chapter 7, pp. 127–135. Pergamon Press, Oxford (1970).
2. G. L. Shires, A. R. Pickering and P. T. Blacker, Film cooling of vertical fuel rods, *AEEW*-R343 (1964).
3. G. F. Hewitt, H. A. Kearsey, P. M. C. Lacey and D. J. Pulling, Burnout and nucleation in climbing film flow, *Int. J. Heat Mass Transfer* **8**, 793–814 (1965).
4. T. Fujita and T. Ueda, Heat transfer to falling liquid films and film breakdown—I. Subcooled liquid films, *Int. J. Heat Mass Transfer* **21**, 97–108 (1978).
5. T. Sato and H. Matsumura, On the conditions of incipient subcooled-boiling with forced convection, *Trans. Japan. Soc. Mech. Engrs* **29**(204), 1367–1373 (1963).
6. A. E. Bergles and W. H. Rohsenow, The determination of forced-convection surface-boiling heat transfer, *J. Heat Transfer* **86**, 365–372 (1964).
7. S. Toda and H. Uchida, A study of liquid-film-cooling with evaporation and boiling, *Trans. Japan. Soc. Mech. Engrs* **38**(311), 1830–1837 (1972).
8. W. H. McAdams *et al.*, Heat transfer at high rates to water with surface boiling, *Ind. Engng Chem.* **41**, 1945–1955 (1949).
9. K. Nishikawa, Heat transfer in nucleate boiling, *Trans. Japan. Soc. Mech. Engrs* **22**(120), 557–561 (1956).
10. K. R. Chun and R. A. Seban, Heat transfer to evaporating liquid films, *J. Heat transfer* **93**(4), 391–396 (1971).
11. V. I. Petrovichev, L. S. Kokorev, A. Ya. Didenko and G. P. Dubvrovskiy, Droplet entrainment in boiling of thin liquid films, *Heat Transfer—Soviet Res.* **3**(1), 19–22 (1971).
12. T. Ueda and T. Tanaka, Studies of liquid film flow in two-phase annular and annular-mist flow regimes (Part 1, Downflow in a vertical tube), *Bull. J.S.M.E.* **17**(107), 603–613 (1974).
13. M. S. Plesset and S. A. Zwick, The growth of vapour bubbles in superheated liquids, *J. Appl. Phys.* **25**(4), 493–500 (1954).
14. S. J. D. van Stralen, M. S. Sohal, R. Cole and W. M. Sluyter, Bubble growth rates in pure and binary systems: Combined effect of relaxation and evaporation microlayers, *Int. J. Heat mass Transfer* **18**, 453–467 (1975).
15. T. D. Patten and W. A. Turmeau, Some characteristics of nucleate boiling in thin liquid layers, in *Proceedings of the 4th International Heat Transfer Conference*, B2.10, pp. 1–11 (1970).
16. A. B. Ponter, G. A. Davies, T. K. Ross and P. G. Thornley, The influence of mass transfer on liquid film breakdown, *Int. J. Heat Mass Transfer* **10**, 349–359 (1967).
17. D. E. Hartley and W. Murgatroyd, Criteria for the break-up of thin liquid layers flowing isothermally over solid surfaces, *Int. J. Heat Mass Transfer* **7**, 1003–1015 (1964).
18. W. S. Norman and V. McIntyre, Heat transfer to a liquid film on a vertical surface, *Trans. Instn Chem. Engrs* **38**, 301–307 (1960).
19. G. F. Hewitt and P. M. C. Lacey, The breakdown of the liquid film in annular two-phase flow, *Int. J. Heat Mass Transfer* **7** 781–791 (1965).
20. S. Suzuki and T. Ueda, Behaviour of liquid films and flooding in counter-current two-phase flow, JSME 861 Meeting (in Japanese), pp. 33–36 (1975).

TRANSFERT THERMIQUE POUR DES FILMS TOMBANT ET RUPTURE DE FILM—II. FILMS LIQUIDES SATURANTS AVEC EBULLITION NUCLEEE

Résumé— Des expériences concernant l'ébullition utilisent des films d'eau saturante qui tombent le long de la surface intérieure d'un tube appartenant à un espace annulaire verticalement disposé et à pression atmosphérique. On présente les résultats relatifs au coefficient de transfert thermique et au débit de gouttes liquides entraînées par l'ébullition, pour un domaine de flux de chaleur qui s'étend jusqu'à la rupture du film. Tenant compte des caractéristiques du débit de gouttes, on discute de la variation du débit du film liquide le long de la surface chauffée et des conditions de rupture du film.

WÄRMEÜBERGANG AN RIESELFILME UND AUFREIßEN DES FILMS TEIL 2: GESÄTTIGTE FLÜSSIGKEITSFILME MIT BLASENSIEDEN

Zusammenfassung— Zur Bestimmung des Wärmeüberganges an gesättigte Wasserfilme am inneren Rohr eines vertikalen Ringspaltes bei Atmosphärendruck wurde eine Reihe von Versuchen durchgeführt. Es werden Werte für Wärmeübergangskoeffizienten und Flüssigkeits-Tröpfchenabscheidu g durch Blasensieden für einen Bereich der Wärmestromdichte bis zum Aufreißen des Filmes angegeben. Unter Berücksichtigung der Charakteristik der Tröpfchenrate werden die Variation ker Rieselmenge entland der Heizfläche und die Bedingungen des Filmaufreißens diskutiert.

ПЕРЕНОС ТЕПЛА К СТЕКАЮЩИМ ПЛЕНКАМ ЖИДКОСТИ И РАЗРУШЕНИЕ ПЛЕНКИ — 2. ПЛЕНОЧНОЕ ТЕЧЕНИЕ НАСЫЩЕННОЙ ЖИДКОСТИ ПРИ ПУЗЫРЬКОВОМ КИПЕНИИ

Аннотация — Проведено экспериментальное исследование процесса теплообмена при пленочном течении насыщенной жидкости вниз по внутренней поверхности вертикальной трубы при атмосферном давлении. Представлены результаты по определению коэффициента теплообмена и скорости осаждения капель при кипении в области докритических тепловых потоков. Проанализированы изменение скорости течения пленки на нагреваемой поверхности и условия возникновения критического режима с учетом скорости капель.